Highlights from the 2011 CASA Infrasound Field Experiment

David Pepyne and Sean Klaiber

22 February 2012

1. Introduction

Each year tornadoes cause property damage and death, some of which might be avoided by providing the public with increased warning lead-time. Several years of field studies by NOAA through its ISNet project showed that tornadoes and their precursors generate infrasound in the 0.5 to 10 Hz frequency band (Bedard et al., 2004a). The ISNet project also showed that precursors to tornadoes can sometimes be detected some 30 minutes or more prior to vortex touchdown (Bedard et al., 2004b). Given that the average tornado warning lead-time in the U.S. is currently ~13 minutes (http://www.noaa.gov/features/protecting/tornados101.html), these results have led to the conjecture that passive remote sensing of infrasound has the potential to improve tornado warning lead-time.[1]

Of course to realize this potential of increasing tornado early warning lead-time, infrasound installations capable of robust and reliable operation in all weather conditions are necessary. Specifically, for tornado early warning, the infrasound site making the detection can be located no more than a maximum of about 100 km from the tornado. Any further and the detection is not useful for early warning due to the relatively slow speed of sound – for sound, 100 km is approximately 5 minutes propagation time. What this means is that the infrasound site must be able to give reliable detection and localization of infrasound signals coming from supercells that are either quite close, or in fact, directly over the top of the infrasound site itself.

As an adjunct to its research related to dense networks of rapid-scan, high-resolution boundary layer observing X-band radars (McLaughlin et al., 2009), the Center for Collaborative Adaptive Sensing of the Atmosphere (CASA) has launched a pilot study to understand the various ways that infrasound might be integrated into the weather prediction, forecasting, warning, and response infrastructure. The first field experiment under this pilot study was conducted in the spring of 2011. The goals of the field experiment were to understand issues related to the design, deployment, and operation of infrasound sites for the monitoring of infrasound from severe convective storms. The purpose of this paper is to describe the experiment, present the main results, and discuss how the lessons learned from the results will be incorporated into a planned 2012 re-deployment.

AFFILIATIONS: Pepyne and Klaiber are with the NSF Engineering Research Center for Collaborative Adaptive Sensing of the Atmosphere at the University of Massachusetts, Amherst, Massachusetts.
CORRESPONDING AUTHOR: David Pepyne, University of Massachusetts, 151 Holdsworth Way, Amherst, MA 01003. E-mail: pepyne@ecs.umass.edu.

[1] There is evidence from researchers studying public response that 30 minutes may be the "ideal" tornado warning lead time (Hoekstra et al., 2011).

2. Experiment Setup

For CASA's first ever infrasound data collection field experiment, two essentially identical infrasound monitoring sites were deployed during the 2011 springtime tornado season. As shown in Figure 1, one site was collocated with the CASA radar in Cyril, Oklahoma, and the other with the CASA radar in Rush Springs, Oklahoma.[2] The two infrasound sites were in place from 18 April 2011 to 27 June 2011.

Figure 1. Locations of the two 2011 CASA infrasound monitoring stations along U.S. Route 44 in Southwestern Oklahoma. One site was collocated with the CASA radar in Cyril, Oklahoma. The other site was collocated with the CASA radar in Rush Springs, Oklahoma. The Cyril site was designated KCYR. The Rush Springs site was designated KRSP.

Each of the infrasound sites used four Paroscientific Model 6000-16B digital nano-barometers. In addition to providing calibration standard, temperature compensated absolute barometric pressure measurements, these instruments have a "nano-resolution" mode that allows them to detect the entire range of atmospheric infrasound, from the very lowest frequencies to the very highest (Schaad, 2009). The four barometers were arranged to form an array with an approximate square aperture measuring roughly 50 meters on a side, as illustrated in Figure 2. Sensor arrays are needed for the weather hazard early warning application so that the infrasound arrival direction (bearing) and apparent horizontal velocity can be estimated as an aid to localizing and identifying different infrasound emitters.

[2] The CASA radars were deployed in Oklahoma from 2006-2011. They have since been removed from Oklahoma for redeployment in the Dallas-Fort-Worth metroplex region, where they will be used both operationally and for research related to, for example, urban tornadoes, urban flooding, convective storm initiation, and air quality studies. The re-deployment is expected to be complete by the end of 2012.

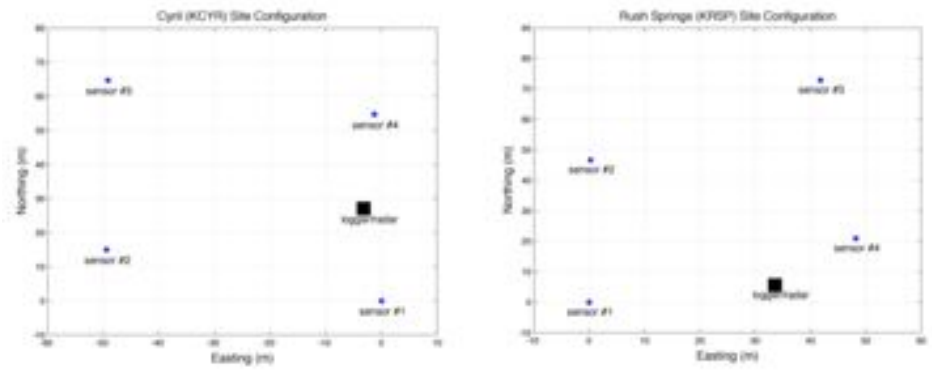

Figure 2. Sensor array configurations at the two infrasound sites, Cyril on the left, Rush Springs on the right. The dots are the sensor locations. The squares are the locations of the CASA radar tower and equipment building where the data logger computers were located.

Each barometer was protected inside a weather-tight hardware store paint bucket "vault" that was partially buried and ballasted with pea stones. Sprinkled on the pea stones was a desiccant powder to remove any moisture that might get inside the bucket. Coming out of the bucket was a data cable and a pressure hose. The data cable was run underground back to a data logger computer in the CASA radar equipment building. The data logger computer was placed inside the CASA equipment building so it could be plugged in to the electrical power and high-bandwidth Internet connection in place there for the CASA radars. The pressure hose was connected to a summing manifold made out of plastic plumbing parts to an 8-arm, 15-meter (50-foot) diameter "soaker hose" spatial wind filter, two examples of which are shown in Figure 3. Such spatial wind filters, consisting of a circularly symmetric arrangement of soaker hoses or pipes, are the current standard for wind noise reduction in infrasound applications (Walker and Hedlin, 2010). Spatial wind filters work by summing the pressure contributions over a large physically distributed area. By doing so SNR is increased due to the fact that infrasound signals passing over the area covered by the filter are coherent over many 100's of meters and hence sum constructively in the summing manifold, whereas the pressure fluctuations due to wind noise become incoherent over a few meters and hence sum destructively in the summing manifold. Circular symmetry makes the spatial wind filter omnidirectional, i.e., such that its filtering performance does not depend on the wind direction.

Figure 3. Close-up of a sensor installation at the Cyril infrasound site (left) and Rush Springs infrasound site (right).

Wind filtered pressure data was collected for 71 days, from 18 April 2011 to 27 June 2011, at a sample rate of 20 Hz.[3] A human readable XML-like data format was used for data logging (storage). Figure 4 shows the header and first few samples from a typical data file: the header gives information about the sensor locations and the barometer configuration parameters, each sample contains the sample index, sample time, and the pressure data from each of the four barometers at the site. Here we note the use of a single time-stamp for all four pressure measurements. A single time-stamp could be used since the four barometers at a site were controlled by a single data logger computer. In this setup, it is only the relative times between samples that needs to be precise rather than the absolute clock times associated with the sample instants. Measurements showed a sample period accuracy better than 10^{-5} seconds. The use of the internet network time protocol kept the absolute clock times accurate to within a few seconds. See (Pepyne et al., 2011) for details regarding the design and operation of the data loggers. In addition to pressure, 20 days of wind speed and direction data were recorded at the Cyril site using a Vaisala WXT510 Weather Transmitter (www.vaisala.com) at a sample rate of 0.1 Hz. Similar to the pressure data, the wind data was stored in a human-readable XML-like format.

[3] The Rush Springs site had several data cable breakages due to cows on the site and so ran with only three sensors for much of the experiment. During the last few weeks of the experiment only two sensors were working at the Rush Springs site. With only two sensors, unambiguous bearing estimation is not possible. The Cyril site, in contrast, operated flawlessly with all four sensors for the entire 71 day data collection period.

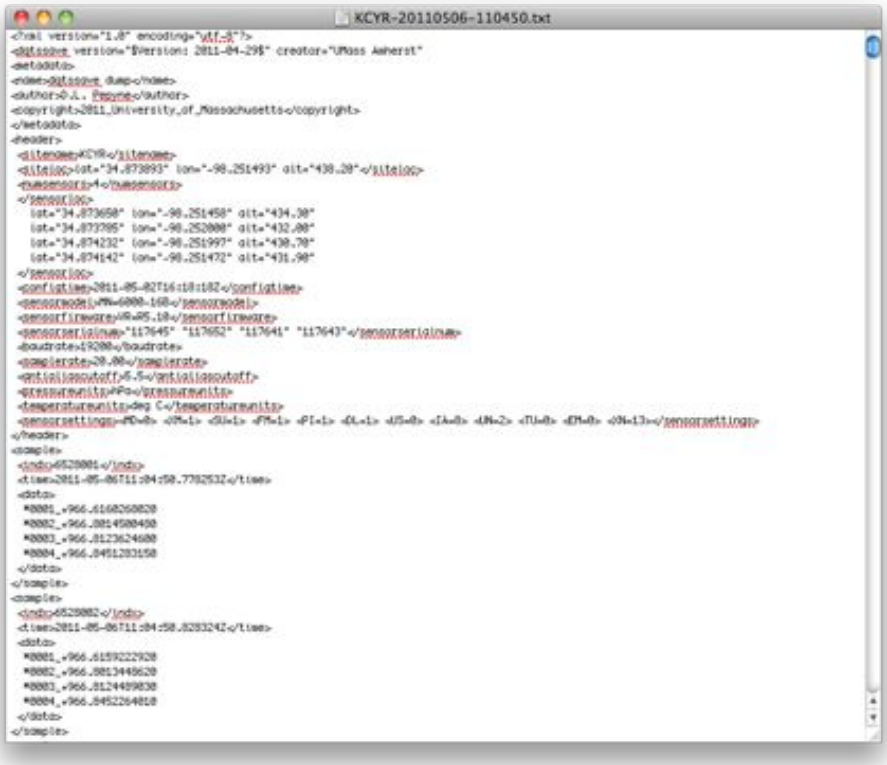

Figure 4. Example pressure data file from the Cyril (KCYR) infrasound site. Each file starts with a header giving the sensor locations and the configuration of the barometers at the site. The header is followed by 5-minutes of pressure samples (at 20Hz this amounts to 6000 samples per file). Each pressure sample has a unique sample index, a time stamp, and the pressure values from the four barometers at the site.

3. Data Analysis

The Paroscientific barometer is a digital instrument generating pressure samples directly in units of hPa (hectopascal, 1 hPa = 100 Pa) over a serial data cable.[4] Each pressure sample, x, can be decomposed into the following components,

$$x = \text{bias} + \text{trend} + \text{infrasound} + \text{residual\_wind} + \text{sensor\_noise} \qquad (1)$$

Bias and trend represent the barometric pressure and its slow change over time. Since our lower frequency of interest is 0.5 Hz, we define trend as any variation in pressure that occurs at a rate of less this frequency. The residual wind is the noise due to wind that is not removed by the spatial wind filters. Sensor noise is the noise internal to the sensors due thermal effects, digital round-off, and forth.

[4] The pressure units as well as almost everything else about the barometer's operation is user configurable (Paroscientific, Inc. Digiquartz Pressure Instrumentation, User's Manual for Digiquartz Broadband Intelligent Instruments with Dual RS-232 and RS-485 Interfacing, Document No. 8819-001, Rev. P, March 2009).

Regarding infrasound signals, they can be classified as either impulsive or periodic. Examples of impulsive infrasound signals include those from explosions, sonic booms, and meteors entering the atmosphere. Impulsive signals typically have relatively short duration, a single pressure spike followed by a period of atmospheric relaxation. In contrast to impulsive infrasound signals, periodic infrasound signals are narrowband or wideband signals that persist for several minutes to several hours or even days. The vortices associated with tornadoes emit wideband periodic signals; other examples of periodic infrasound signals include mountain waves due to wind passing over mountainous terrain and microbaroms due to ocean swells (Crocker, 1997).

To capture signals in the 0.5 to 5.0 Hz frequency band associated with large and medium vortices (Bedard et al, 2004a), the analysis in this paper is based on the use of analysis windows ranging in size from 1024 samples (1024 samples at 20 Hz represents approximately 1-minute of data collection) to 6000 samples (5-minutes of data collection). Because the bias due to the ambient barometric pressure is so much larger than the infrasound signals of interest – barometric pressure is on the order of 1000 hPa vs. 0.001 hPa or less for infrasound signals from tornadoes (Crocker, 1997) – our first data processing step is to remove the bias. This involves calculating the mean of x over the data analysis window and subtracting this mean value from each sample. Low frequency trends are then removed by high-pass filtering with a filter with a low-frequency cutoff of 0.1 Hz. High frequencies above 5.5Hz are removed by the anti-aliasing filters inside the barometers.[5]

After bias and trend removal, each pressure sample has the form,

$$x = \text{infrasound}(s) + \text{residual\_wind} \qquad (2)$$

Here we ignore the sensor noise, since as we will see, it is dominated by the residual wind noise, and hence has no practical impact on the results to be presented. The '(s)' on infrasound is included to acknowledge that, in general, there can be multiple infrasound sources emitting at the same time. The plots in Figure 5 show traces of raw pressure, mean removed pressure, and band-pass filtered pressure.

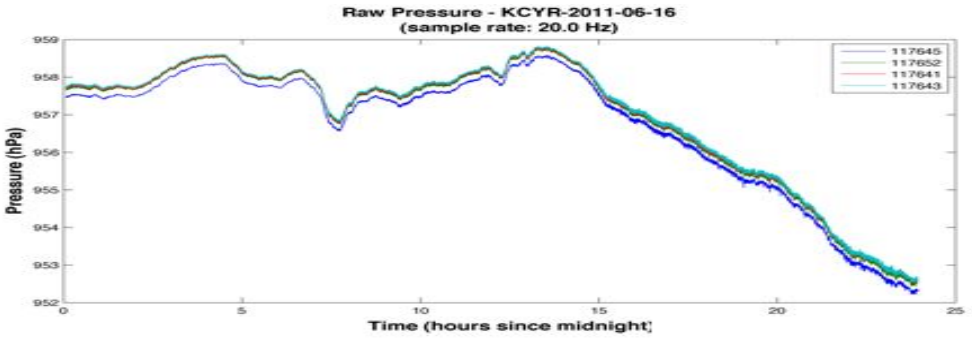

[5] The barometer anti-alias filter cutoff frequency is user selectable using the barometer's IA command. For the complete list of barometer configuration settings, see the '<sensorsettings>' line in the example data file in Figure 4.

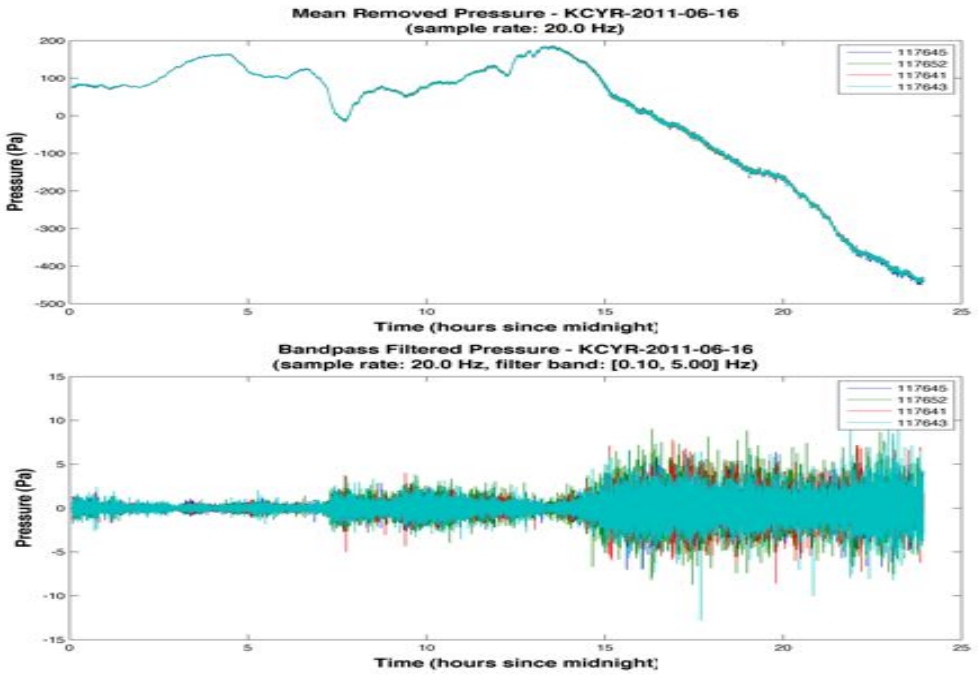

Figure 5. Plots showing typical values of the raw pressures (top), the pressures after bias removal (middle), and the pressures after band-pass filtering (bottom).

For sensors less than a few kilometers apart, the infrasound(s) will be correlated sensor-to-sensor, this is the Mack-Flinn model (Mack and Flinn, 1971). For sensors more than a few 10's of meters apart, the residual wind noises will be uncorrelated sensor-to-sensor. This is the property that forms the basis of the spatial wind filter, e.g., (Walker and Hedlin, 2010). Thus, for a signal, x, decomposed as in Equation (2), two plots are particularly useful in summarizing a data set that potentially contains periodic infrasound signals. The first are daily *spectrogram* plots from each sensor. In a spectrogram plot, the horizontal axis is time-of-day, the vertical axis is frequency, and the colors represent the spectral power at each frequency at each time. The second set of plots are daily *cohereogram* plots.[6] For the cohereogram plots, the horizontal axis is again the time-of-day, the vertical axis is frequency, but for this plot the color represents the average magnitude squared coherence of all sensor pairs. This is a number between 0 and 1: 0 meaning no correlation at a given frequency; 1 meaning perfect linear correlation at that frequency. Considered together these plots are interpreted as follows. Periodic infrasound signal(s) passing over an array would be revealed by high coherence at a specific set of frequencies that also appear in the spectrogram of each sensor. Absence of infrasound signal(s) would be revealed by low coherence and low spectral power at all frequencies in the sensor spectrograms. Excessive noise would, such as that due to wind, be revealed by a combination of low coherence and high spectral power over a wide band of frequencies in the sensor spectrograms. With this in mind, Figure 6 plots a sensor spectrogram, the corresponding array

[6] The cohereogram is a plot of coherence vs. time. Coherence is a measure of the linear correlation of two power spectra (Chatfield, 2004). We obtain our coherence plots by averaging the magnitude squared coherence over all unique sensor pairs. With N sensors, there are $N(N-1)/2$ such pairs. For a four sensor array, these include pairs 1-2, 1-3, 1-4, 2-3, 2-4, and 3-4.

cohereogram, and the associated wind speed as recorded at the Cyril site on 16 June 2011. As seen in the plots, where the wind speed is low there is a nearly continuous infrasound signal with a very characteristic signature consisting of a fundamental just below 1 Hz and harmonics at intervals of approximately every 1 Hz above the fundamental. On the other hand, where the wind speed is high, coherence is lost across the array and "blooms" of wideband spectral power are observed in the sensor spectrograms.

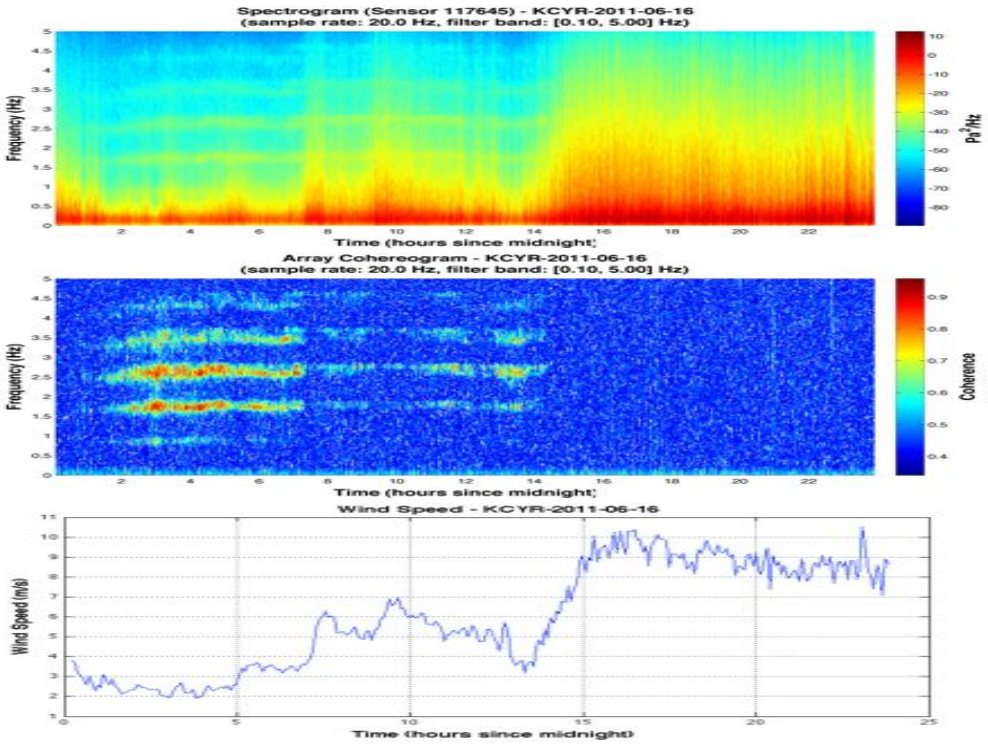

Figure 6. Sensor spectrograms (only one of the sensors is shown, the other two are similar), the corresponding array cohereogram, and the associated wind speed recorded at the Cyril site on 16 June 2011.

4. Results

4.1 *Wind Filter Performance*

Assuming the infrasound signal in Figure 6 continues throughout the entire day, then it is clear that our ability to detect it depends on the wind speed. Comparing the wind speed plot to the coherence plot in Figure 6, we can estimate by eye the wind speed above which we can no longer detect the infrasound signal to be about 5 m/s. The reason for the loss of detection would seem to be the increase in spectral power with increasing wind speed. Since the increase in spectral power increases first at the low frequencies and moves into increasingly higher frequencies as the wind speed increases, we first lose the ability to detect the low frequencies, followed by the high frequencies with increasing wind speed.

In an effort to characterize the relationship between the wind speed and the power spectrum, Figure 7 plots the wind speed against the maximum frequency above which the power spectrum from sensor 1 never again exceeds a threshold of -20 dB. This threshold criterion was chosen in an ad hoc way by eye from the spectrogram plot as a sort of "edge detector" to track the transition region where the spectrogram goes from red to yellow (this occurs between -30 and -20 dB). Also shown in Figure 7 is a scatter plot of wind speed vs. the -20dB threshold frequency. These curves along with a correlation coefficient of 0.96 reveal a strong linear relationship between the two quantities.

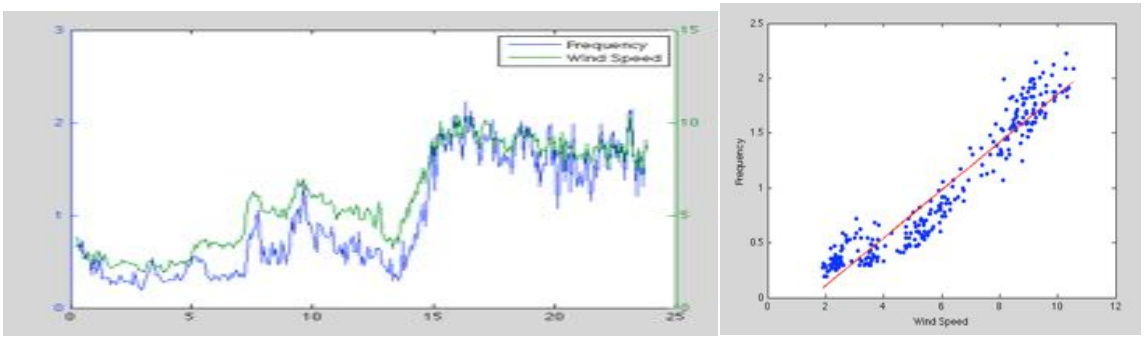

Figure 7. Overlaid plot of wind speed and the frequency above which the power spectrum (sensor 1) never again exceeds a threshold of -20 dB, and scatter plot relating the two.

Another effect of wind noise entering the spatial wind filters is seen by comparing the wind speed plot in Figure 6 to the plot of the filtered pressure in Figure 5. Here we see a clear correlation between increasing wind speed and increasing amplitude of the filtered signal. One summary measure of amplitude excursions is the RMS pressure. This is the square root of the mean of the squares of the pressure samples over the given analysis window. Figure 8 compares the wind speed against RMS pressure. The scatter plot in Figure 8 again shows a strong linear relationship, the correlation coefficient in this case is 0.93.

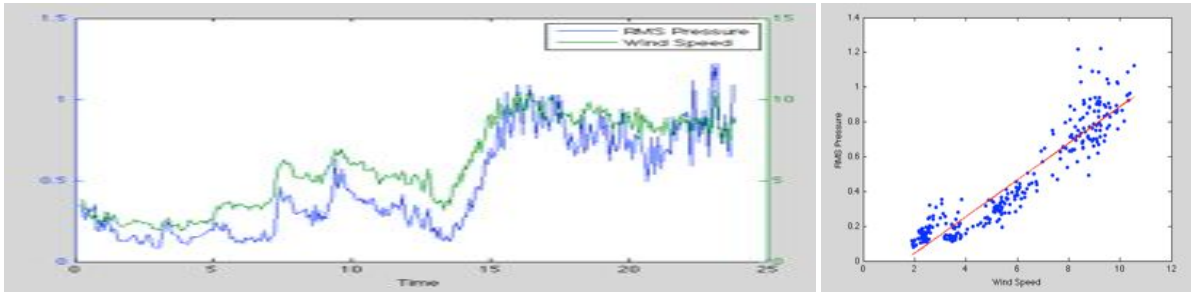

Figure 8. Plot of wind speed overlaid with RMS pressure, and scatter plot showing the relationship between the two.

Using the coefficients of the linear regression in Figure 7, we can obtain an expression that allows us to infer the wind speed from the spectrogram data. In particular, the equation relating wind speed, w (m/s), to -20dB threshold frequency, f (Hz), is,

$$f = 0.2181w - 0.3264$$

leading to,

$$w = (f + 0.3264) / 0.2181. \qquad (3)$$

As a quick and dirty estimate of wind speed, f in Equation (3) is the frequency where a spectrogram plot transitions from red to yellow. Figure 9 shows a typical 5 days of spectrogram data from the Cyril infrasound site. Using Equation (3), we can conclude that the local wind speed exceeded the 5 m/s detection threshold for more than half of the time – consistently during the daylight hours from 12 UTC to 24 UTC (7AM to 7PM local).

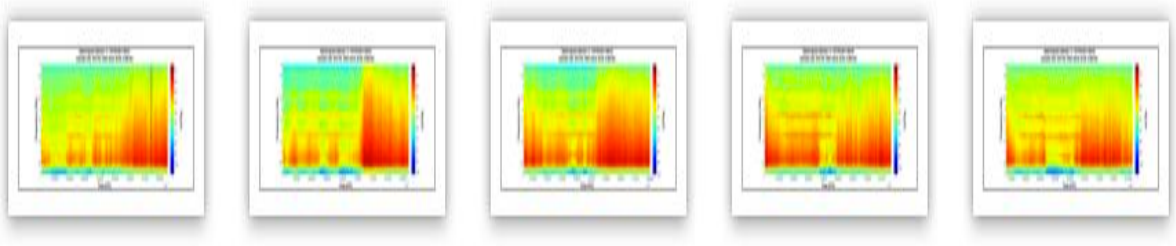

Figure 9. Five days of typical spectrograms from sensor 1 at the Cyril site.

Using the 20 days of data collected at the Cyril site from 02 June 2011 to 21 June 2011, the plot in Figure 10 shows the median wind speed for each hour of the day. This plot confirms our above analysis that the wind speeds exceed 5 m/s over much of the day, but particularly between the daylight periods of 12 UTC to 24 UTC (7AM to 7PM local).[7]

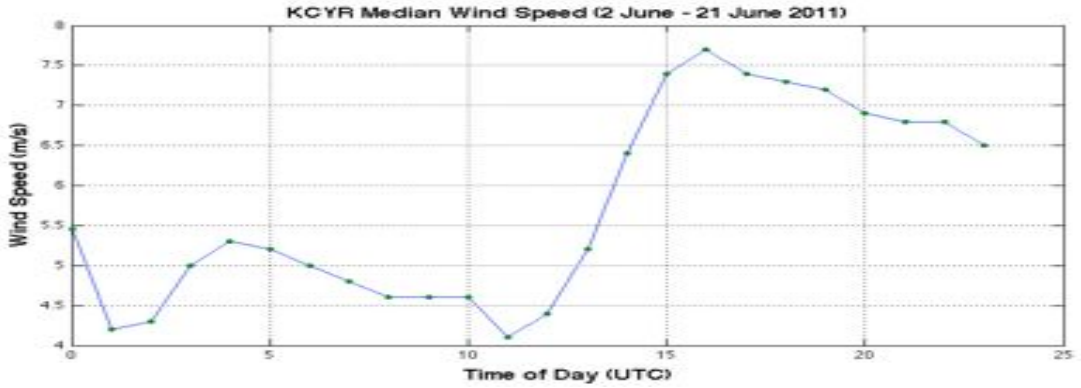

Figure 10. Median wind speed throughout the day at the Cyril site for the 20 day period 02 June – 21 June 2011.

[7] Note we do not examine the wind direction, since our wind filters are designed to be omnidirectional and hence their performance should not be a function of wind direction.

4.2 *Persistent Infrasound Clutter*

Turning now to the continuous infrasound signal in Figure 6, a spectral analysis of the 71 days of data collected during the field experiment shows that this characteristic signal was present nearly all the time that there was not excessive wind noise contamination. Moreover, the signal was present not only at the Cyril site, but also at the Rush Springs site. This is illustrated in Figure 11, which shows the cohereograms for a typical 5 days from each of the two sites.

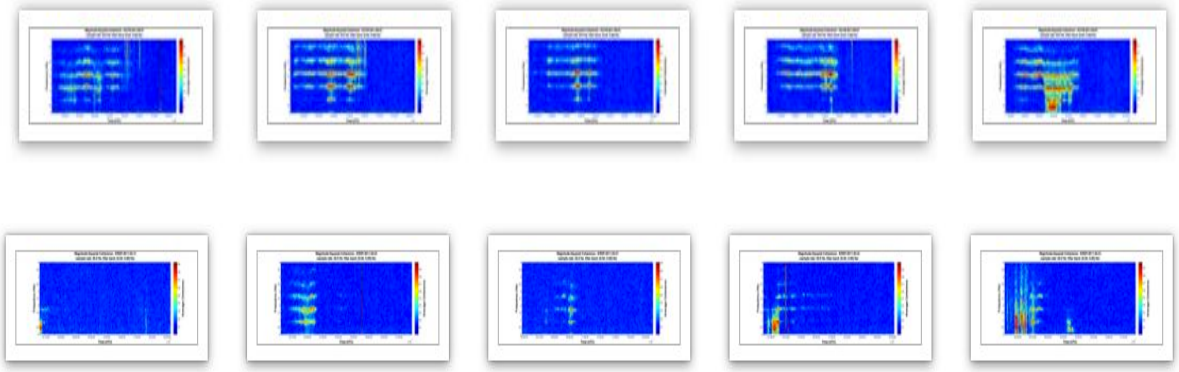

Figure 11. Typical cohereograms from the Cyril (top) and Rush Springs (bottom) infrasound sites showing detection of an infrasound signal with very characteristic coherence signature nearly all the time that the wind noise was not excessive.

It is of interest to try to determine the source of this persistent infrasound signal. Assuming the infrasound source is sufficiently far from the site (a few 10's of wavelengths is sufficient), the infrasound signal passes over the infrasound array as a planar wavefront. In this case, each wavefront will arrive at each sensor at a slightly different time. From the arrival times at each sensor we can estimate the azimuth (bearing) direction pointing back to the signal source. In particular (see (Olson and Szuberla, 2004) for details), if we let *R* be the relative position matrix of each sensor pair *i* and *j*,[8] *TDE* be the vector of arrival times of the infrasound wavefronts at each sensor pair, and define,[9]

$$U = \begin{bmatrix} U_x \\ U_y \end{bmatrix} = \left(\frac{1}{V}\right)\begin{bmatrix} \sin(\theta) \\ \cos(\theta) \end{bmatrix}$$

then,

[8] Again, with N sensors there are N(N – 1)/2 unique sensor pairs.

[9] Here we give the 2D definition of U. In the 2D definition, V is the so-called "apparent horizontal velocity" of the wavefront across the plane of the array. This velocity, obviously depends on the elevation angle from which the wavefront is arriving from. An elevated source, or a wave that has been ducted through the atmospheric waveguide, cf (Drob, 2003), will have a higher apparent horizontal velocity. A full 3D expression for U includes elevation angle and is given in (Rost and Thomas, 2002).

$$TDE = R\ U$$

which implies,

$$U = (R\ R^{T})^{-1}\ R^{T}\ TDE \qquad (4)$$

where we use a pseudo-inverse to account for the matrix R not being square. Given U,

$$\theta = \tan^{-1}(U_x, U_y)$$

and

$$V = 1/\mathrm{sqrt}(U_x^2 + U_y^2).$$

where θ is the bearing angle pointing back to the infrasound source and V is the apparent horizontal velocity of the infrasound wavefronts.

The relative arrival times of the infrasound wavefronts between the sensor pairs that provide the input to the bearing estimation algorithm in Equation (4), can be estimated from the lag associated with the peak of the cross-correlation function (xcorr), i.e.,

$$TDE_{ij} = -\mathrm{argmax}(\ \mathrm{xcorr}(x_i, x_j)\ )\ /\ Fs$$

where x_i and x_j are vectors of pressure signals from sensors i and j respectively (we use 1-minute blocks of pressure data for the cross-correlation calculation), and Fs is the sample rate in Hz (20 Hz in our case). Since the cross-correlation function is a discrete function with resolution equal to the sample period, curve fitting is generally used in order to obtain subsample resolution. For the analysis here, we used a polynomial curve fit around the cross-correlation peak.

One caution when using cross-correlation to estimate time-delays is that the technique can give misleading results when the input is a mixture of signals from multiple emitters. The usual way to try to separate multiple sources is to pre-process the pressure data through a narrow band-pass filter prior to the application of the bearing estimation algorithm. This works except where the spectra of the two signals overlap. While typically a fixed set of filter passbands are used (e.g., Brachet et al., 2010), we chose our filter passband specifically to include the frequency components of the continuous infrasound signal. For the Cyril site, both the 0.5 to 1.5 Hz and 1.5 to 3.0 Hz passbands gave very consistent bearing and velocity results, as seen from the plots in Figure 12.

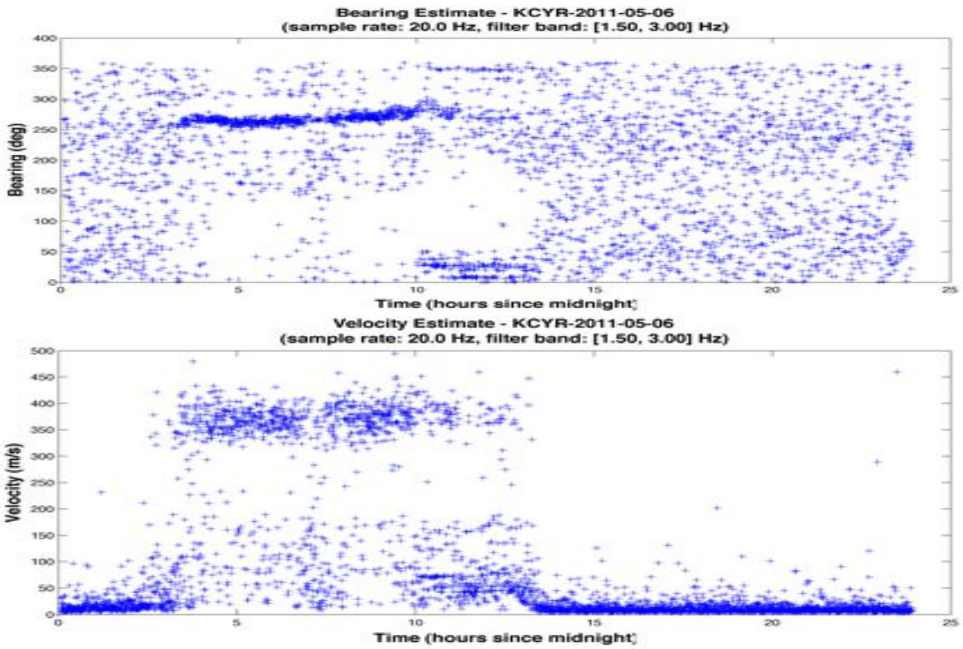

Figure 12. Bearing angle and velocity plots for the persistent infrasound signal form the Cyril site.

The best results for the Rush Springs site were obtained with a 0.5 to 3.0 Hz passband. One issue with the Rush Springs site, however, was that the signal was much weaker there. When the signal-to-noise (SNR) is low, the cross-correlation function can give misleading time-delay estimates. In particular, because the variance of the cross-correlation estimate increases with lag, spurious large time-delays become more common. At the Rush Springs site, these led to the appearance of detections coming from certain very specific directions as shown in the top plot in Figure 13. One indicator that these are false detections is the band of very low velocities throughout the velocity plot shown in the bottom plot in Figure 13.

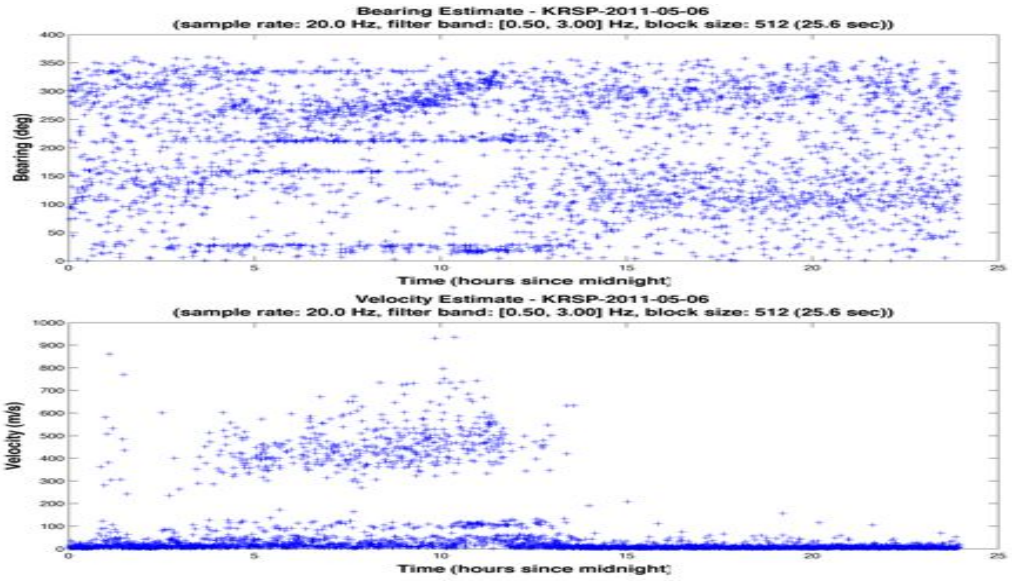

Figure 13. False bearing angles (top) and low velocities (bottom) at the Rush Springs site due to poor performance of cross-correlation time-delay estimation resulting from low SNR.

Since for a sensor spacing of ~50 m the time for a wavefront to travel between sensors at the nominal speed of sound of 342 m/s is ~0.15 seconds, let us remove all bearing and velocity estimates obtained from time-delay vectors containing time-delays larger than 0.2 seconds. Doing so we get the results in Figure 14.

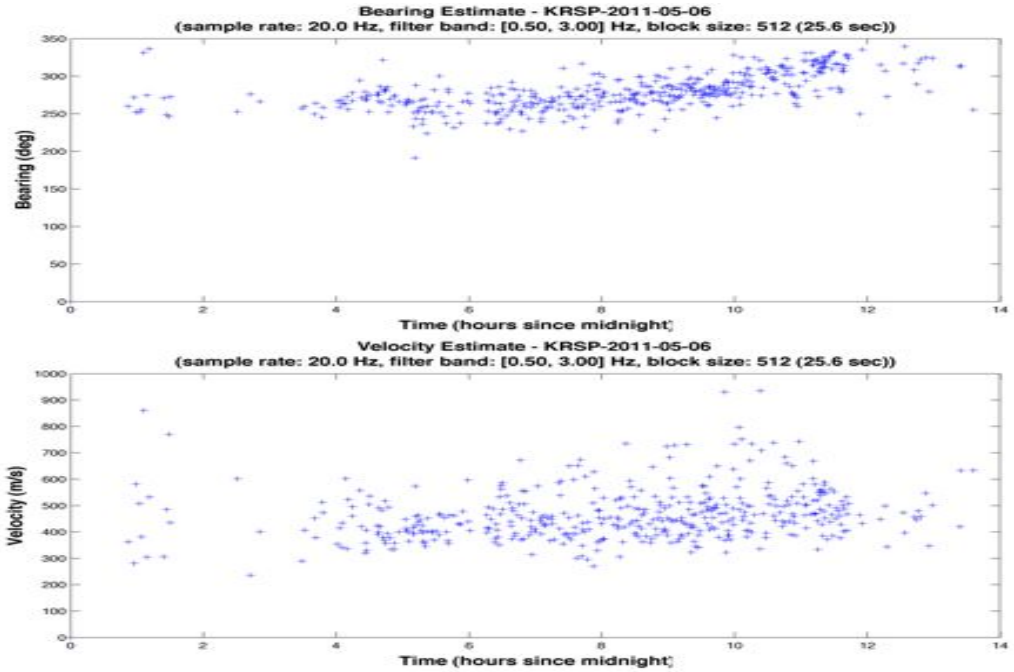

Figure 14. Bearing and velocity estimates for the persistent infrasound signal from the Rush Springs site.

Examining the results, we first note that the velocities estimated at the sites are somewhat higher than the nominal 342 m/s speed of sound. Since the arrays are estimating apparent horizontal velocity, this is expected since the estimated horizontal speed will tend to be higher due to the fact that infrasound from more than a few kilometers away will typically arrive from an elevated angle through the atmospheric waveguide (Drob, 2003).

Regarding the bearing angles, the estimates from the Cyril site are very steady at ~260 degrees, while the estimates from the Rush Springs site, while more dispersed are consistently between 250 and 300 degrees. In any case, it seems evident that (i) the source of the persistent infrasound signal is not moving, (ii) the same coherence spectrum suggests the signal seen at both sites is from the same source, and (iii) the source is located somewhere to the west of both sites, farther from the Rush Springs site than from the Cyril site as indicated by a weaker signal at Rush Springs. Following the bearing angle estimates to the west in Figure 15, we conclude that the source of the signal is with very high likelihood the Blue Canyon Windfarm, the largest wind farm in the state of Oklahoma. From our experience dealing with turbine

clutter in the data from the CASA radars at Cyril and Lawton, we know that the turbines at this wind farm are almost always turning, and hence are clearly capable of emitting the nearly constant infrasound signal observed during the field experiment.

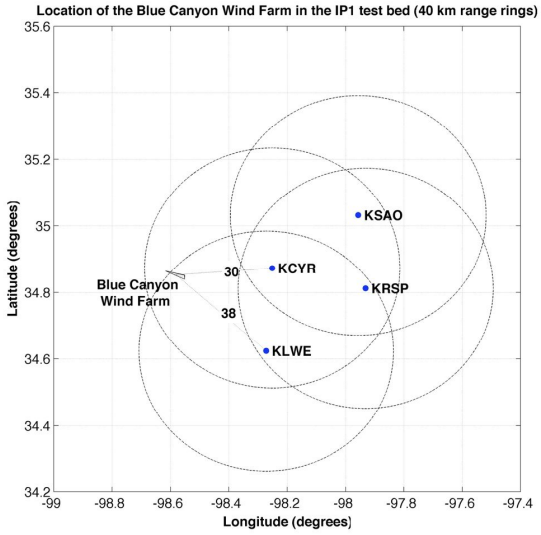

Figure 15. Location of Blue Canyon Windfarm to the west of the infrasound sites, 30 km west of the Cyril site, 60 km west of the Rush Springs site.

4.3 *Tornado Detections*

The 2011 tornado season was a particularly violent and deadly one. In Oklahoma alone, there were 69 tornadoes during the period of our infrasound field experiment (http://www.spc.noaa.gov). For the tornadoes that occurred close to the infrasound sites, such as the EF4 that passed within 30 km of the sites on 24 May, the winds would clearly have exceeded the capabilities of our spatial wind filters, since the infrasound sites would have been under the parent supercell itself. Even for more distant tornadoes, the climatology of Oklahoma is such that tornadoes tend to occur in the early evening hours, when the wind speed tended to exceed the capabilities of our wind filters. Thus, as far as detecting tornadoes, we had very few opportunities due to the ineffectiveness of our wind filters.

One case that we do have occurred a few hours after the 22 May Joplin MO tornado during a period of time when multiple tornadoes were occurring to the east of the infrasound sites. Shown in Figure 16 are the array coherence and bearing estimate plots recorded at the Cyril site over the period 15:00 UTC on 22 May to 09:00 UTC on 23 May (10 AM local Oklahoma time on the 22nd to 1 AM local Oklahoma time on the 23rd). As seen, the coherence shows a period of strong detection at ~24:00 UTC (7 PM local Oklahoma time) with bearing angles pointing generally to the southeast of the sites. One thing to notice is how much different the coherence appears in comparison to the coherence signature from the Blue Canyon wind farm. A forthcoming paper detailing work on our array signal processing techniques will analyze this case in more detail.

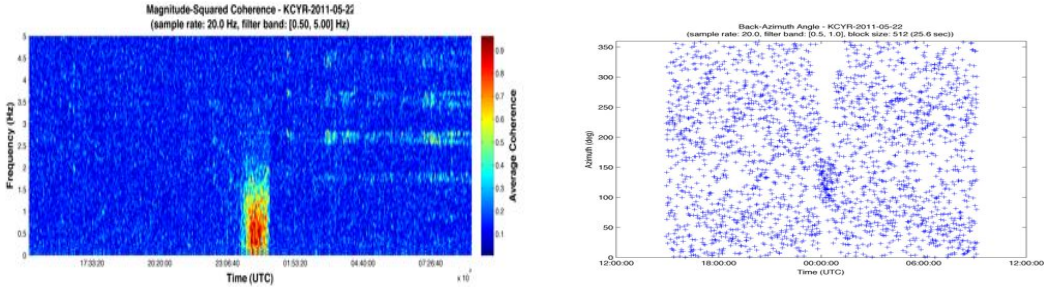

Figure 16. Array coherence (left) and bearing angle estimates (right) recorded on 22 May 2011 at the Cyril site.

5. Summary and Conclusions

This paper described CASA's first ever infrasound experiment to explore the potential of infrasound for the early detection of tornadoes and their precursors. The experiment took place in southwest Oklahoma from 18 April to 27 June 2011. During this period 69 tornadoes occurred in the state of Oklahoma, and may more occurred less than 900 km from the infrasound sites (900 km being the furthest that the ISNet project was able to detect a tornado (Bedard et al., 2004b)).

Unfortunately, ineffective wind filtering rendered almost all of our infrasound data useless for tornado detection. For a relatively strong local infrasound signal, which we traced to the Blue Canyon wind farm, the largest wind farm in the state of Oklahoma, wind speeds above 5 m/s prevented detection. For tornado infrasound, which we expect to be weaker than the wind farm signal, wind speeds less than 5 m/s would be required for detection. Since local wind speeds generally exceed even 5 m/s during the early evening hours when tornadoes in Oklahoma tend to occur, we had very few tornado detection opportunities. The one strong case that we did get on the 22nd of May is being used as a test case for a forthcoming paper on our work on array signal processing techniques.

The main lesson from the experiment is the need for much more effective wind filtering. We suspected, based on the experiences of the NOAA ISNet researchers (Bedard et al., 2004b), that our soaker hose spatial wind filters were not going to be the perfect solution, but we did not expect them to perform so poorly. Whereas our filters were effective to a few m/s, we needed wind filters able to filter to at least the median observed wind speed of just under 8 m/s (recall Figure 10). Ideally, we would like filters able to handle the maximum wind speed of 20 m/s observed by the wind gauge at the Cyril site.

Based on their effectiveness in the NOAA ISNet project, the major change for our proposed 2012 infrasound re-deployment will be the addition of eddy fences. The ISNet researchers had "no signals obscured by wind noise after the installation of the eddy fences" (Bedard et al., 2004b). The eddy fences even allowed an ISNet site to detect and track a tornado that passed

within 3 km of the site (Bedard et al., 2004a). As shown in Figure 17, an eddy fence is a circular fence installed around each spatial wind filter. What an eddy fence does is it raises the boundary layer turbulence up off the ground and then breaks them up to make them smaller and weaker by the time they get to ground level. These smaller, weaker turbulence eddies make the spatial wind filter more effective. The design that we will use will be built from the plans created by Dr. Bedard for the ISNet project. Other changes to the wind filters will be the use of 12 rather than 8 arms. We will still use a 50 foot diameter filter, but we will fold the arms back on themselves, the idea being to make the spatial wind filter more effective by covering more area on the ground.

Figure 17. Eddy fences at the abandoned NOAA ISNet site at the Boulder Atmospheric Observatory (BAO) in Colorado.

The persistent infrasound from the Blue Canyon wind farm was another interesting finding. Not only does such a finding have implications with respect to possible effects of infrasound on people living near wind farms, particularly given that the infrasound signals could be detected some 60 km from the wind farm, the finding also has implications with regard to array signal processing. As the number of facilities such as wind farms continues to increase, we will have to expect that there will be human-made infrasound signals present that will interfere with the detection of the natural infrasound signals of interest. That is, when searching for tornadoes, the infrasound from a wind farm is clutter that we will have to differentiate from any tornado detections. While there are array signal processing techniques that can do this signal separation (cf (Krim and Viberg, 1996; Rost and Thomas, 2002; Swanson, 2012)), the challenge that we are exploring for a forthcoming paper (Pepyne, 2012) is coming up with a technique that can do this while at the same time is able to detect low SNR signals and give good bearing angle accuracy over a wide band of frequencies with as few as four sensors. Keeping the number of sensors to a minimum is to keep costs and land use to a minimum, and is particularly necessary for infrasound applications, like severe weather monitoring, that require eddy fences.

In closing, we hope to return next year with much better results to report.

Acknowledgements

CASA is supported primarily by the Engineering Research Centers program of the National Science Foundation (NSF) under NSF Cooperative Agreement EEC-0313747. Funding for this work is provided by the Jerome M. Paros Fund for Measurement and Environmental Sciences Research.

The authors also thank Jerry Brotzge, Mike Zink, Eric Knapp, Eric Lyons for their help in designing and setting up the infrasound sites, and REU students Alex Mendes, Brian McCarthy, and B. Benito-Figueroa who designed and built the data logger computers. The first author also thanks Dr. Al Bedard Jr. for his advice on wind filtering and access to his eddy fence assembly instructions.

References

Bedard, A. Jr., and coauthors, 2004a: The Infrasound Network (ISNET): Background, design details, and display capabilities as an 88D adjunct tornado detection tool. *Proceedings of the 22nd Conference on Severe Local Storms*, 4-8 October 2004, Hyannis, MA. Sponsored by the American Meteorological Society, Boston, MA.

Bedard, A. Jr., and coauthors, 2004b: Overview of the ISNET data set and conclusions and recommendations from a March 2004 Workshop to review the ISNET data. *Proceedings of the 22nd Conference on Severe Local Storms*, 4-8 October 2004, Hyannis, MA. Sponsored by the American Meteorological Society, Boston, MA.

Chatfield, C., 2004: The Analysis of Time Series: An Introduction (6th ed.). *Chapman and Hall/CRC*.

Crocker, M.J., 1997: Encyclopedia of Acoustics. John Wiley and Sons, New York.

Drob, D.P., 2003: Global Morphology of Infrasound Propagation. J. Geophys Res. – Atmospheres, Vol. 108, No. D21, p. 4860.

Hoekstra, S., R. Riley, K. Klockow, S. Erickson, H. Brooks, and J. Brotzge, 2011: A social perspective of warn on forecast: Ideal tornado warning lead time and the general public's perceptions of weather risks. *Weather, Climate and Society,* in review.

Krim, H., and M. Viberg, 1996: Two Decades of Array Signal Processing Research. *IEEE Signal Processing Magazine*, pp. 67-94.

Mack, H. and E.A. Flinn, 1971: Analysis of the Spectral Coherence of Short-Period Acoustic Gravity Waves in the Atmosphere. *Geophys J R astr Soc*, 26, pp. 255-269.

McLaughlin, D., and coauthors, 2009: Short-Wavelength Technology and the Potential for Distributed Networks of Small Radar Systems. *Bulletin of the American Meteorological Society*, **90** (12), 1797-1817.

Olson, J.V. and C.A.L. Szuberla, 2004: The Least-Squares Estimation of the Azimuth and Velocity of Plane Waves. Inframatics, 6, pp. 8-12.

Pepyne, D., M. Zink, J. Brotzge, E. Knapp, A. Mendes, B. McCarthy, S. Klaiber, and B. Benito-Figueroa, 2011: An Integrated Radar-Infrasound Network for Meteorological Infrasound Detection and Analysis. Proc. of the 91st *American Meteorological Society Annual*

Meeting, 15th *Symposium on Integrated Observing and Assimilation Systems for the Atmosphere, Oceans and Land Surface* (IOAS-AOLS), Seattle, WA, January 2011.

Pepyne, D., 2012: Design and Operation of Infrasound Stations for Hazardous Weather Detection. To appear *European Geosciences Union General Assembly*, Vienna, Austria, April 22-27.

Rost, S. and C. Thomas, "Array Seismology: Methods and Applications," *Reviews of Geophysics*, Vol. 40, No. 3, September 2002.

Schaad, T., 2009: Infrasound Signals Measured with Absolute Nano-Resolution Barometers. Paroscientific Doc. No. G8221, Rev. A.

Swanson, D.C., 2012: Signal Processing for Intelligent Sensor Systems with Matlab (2nd ed). CRC Press.

Walker, K.T. and M.A.H. Hedlin, 2010: A Review of Wind-Noise Reduction Methodologies. In *Infrasound Monitoring for Atmospheric Studies*, Springer, pp. 141-181.